



# Neoproterozoic evolution of northern Gondwana recorded in detrital zircon grains from the Gheshlagh bauxite deposit, Alborz Mountains, Iran Block

Gholam Hossein Shamanian<sup>a,b,\*</sup>, Keiko Hattori<sup>a</sup>

<sup>a</sup> Department of Earth and Environmental Sciences, University of Ottawa, Ottawa, ON K1N 6N5, Canada

<sup>b</sup> Department of Geology, Faculty of Science, Golestan University, Gorgan, Iran



## ARTICLE INFO

### Article history:

Received 6 August 2019

Received in revised form 4 September 2020

Accepted 24 December 2020

Available online 09 February 2021

Handling editor: T. Tsunogae

### Keywords:

Gondwana break-up

Cimmerian Continent

Permian paleoclimate

Arabian-Nubian Shield

Paleozoic paleotopography

## ABSTRACT

When the Cimmerian Continent separated from Gondwana and drifted northward to equatorial latitudes, sedimentary rocks on the continent underwent intense weathering, resulting in the formation of bauxite deposits. Gheshlagh is one such bauxite deposit, located in the Alborz Mountains in northern Iran. The bauxite deposit at Gheshlagh, 12–18 m in thickness with a strike length > 4 km, is hosted by Permian strata and unconformably overlain by Early Triassic limestone. Detrital zircon grains in the bauxite deposit yielded U–Pb ages ranging from 2.5 Ga to 0.5 Ga, with most ages between ca. 0.9 Ga and 0.5 Ga. The detrital zircon grains with age populations between ca. 0.9 Ga and 0.6 Ga are tabular and rounded with sharp oscillatory zoning, and most likely derived from igneous rocks in the northern part of the Arabian-Nubian Shield. The detrital zircon grains with ages of ~1 Ga are long and rounded in shape with slightly obscure growth zoning and probably originated from metamorphic rocks of the Sinai basement in the northernmost part of the shield. Detrital zircon with ages between 1.8 and 2.5 Ga are smoothly rounded in shape with faint internal zoning, suggesting long transport from a metamorphosed source(s), possibly including the Saharan Metacraton, and/or the Kabul Block. The Gheshlagh deposit contains minor needle-like to prismatic-shaped zircon grains, with U–Pb ages ranging from ca. 571 to 521 Ma, corresponding to the timing of the Cadomian magmatic event in northern Gondwana. The occurrence of such proximal sourced zircons at Gheshlagh supports the notion that northern Gondwana was an active margin in response to southward subduction of Prototethys during late Neoproterozoic to Early Cambrian. Our data also suggest that the Cimmerian Continent was still located on the northern margin of Gondwana during deposition of the bauxite protolith in the Permian.

© 2021 International Association for Gondwana Research. Published by Elsevier B.V. All rights reserved.

## 1. Introduction

The opening of Neotethys separated an elongate block of land, the Cimmerian Continent, from Gondwana (Sengör, 1979; Angiolini et al., 2015), which was followed by the northward drift of the continent towards Eurasia (Muttoni et al., 2009a). The drifting and eventual collision of the Cimmerian Continent with Eurasia resulted in the fragmentation of the continent, now recognized as allochthonous terranes in Turkey, Iran, Afghanistan, Tibet, Malay Peninsula, and western China (Ueno, 2003). Despite numerous structural, lithological, geochemical and geochronological studies, the causes and timing of the rifting of the Cimmerian Continent remain controversial (e.g., Berberian and King, 1981; Metcalfe, 2013; Angiolini et al., 2015). Allochthonous terranes, which

were once on the Cimmerian Continent, contain numerous Permian bauxite deposits, including those in Turkey (Haniççi, 2013), Iran (Faramarzi et al., 2013), Pakistan (Ashraf et al., 1972) and Afghanistan (Renaud et al., 2015). The Gheshlagh bauxite deposit is one such deposit, now located in the Alborz Mountains of the northern Iran Block. Since bauxite is a product of intense weathering of rocks (Bárdossy and Aleva, 1990; Bogatyrev et al., 2009), dating of detrital zircon from such deposits can indicate not only ages of the provenances of the protoliths, but also the paleogeography of the area (e.g., Mongelli et al., 2014, 2016; Cai et al., 2015; Wang et al., 2016).

This paper provides the first description of the Gheshlagh bauxite deposit including the occurrence, stratigraphy, and petrography of the bauxite ore, and U–Pb ages of detrital zircon from the deposit. More notably, this is the first paper documenting detrital zircon ages from a bauxite deposit in the Cimmerian Continent. Based on our results, we discuss possible provenances for the protolith of the bauxite deposit, and the geodynamic and paleogeographic evolution of northern Gondwana and the Cimmerian Continent during early to late Paleozoic.

\* Present address for the corresponding author at: Department of Geology, Faculty of Science, Golestan University, Gorgan, Iran, shamanian@yahoo.com

E-mail addresses: gshamani@uottawa.ca, shamanian@yahoo.com (G.H. Shamanian).

## 2. Geological setting

### 2.1. Regional tectonic setting

The study area is located in the Alborz Mountains of the northern part of the Iran Block, which lies along the Tethyan suture between the Eurasian Plate to the north and the Arabian Plate to the south (Fig. 1A). The block was part of the Cimmerian Continent based on the correlation of flora (Ghavidel-Syooki, 1995, 2008), sedimentary facies (Stampfli, 2000), and geochronological data (e.g., Ramezani and Tucker, 2003; Hassanzadeh et al., 2008; Shirdashtzadeh et al., 2018). The continent was separated from northern Gondwana by the opening of Neotethys and drifted northward during shortening of the Paleotethys by its subduction below Eurasia. The Cimmerian Continent eventually collided with southern Eurasia to form several allochthonous terranes in present-day Turkey, Transcaucasia, central Iran, southern Afghanistan, Myanmar, western China, and western Thailand to Sumatra (Ueno, 2003; Muttoni et al., 2009b).

### 2.2. Geology of the Alborz Mountains

The Alborz Mountains, a mountain chain over 1200 km long, extends along the western and entire southern coast of the Caspian Sea (Fig. 1A). The oldest exposed unit in the Alborz Mountains consists of siliciclastic and carbonate-dominated sequences, including the Kahar Formation of late Neoproterozoic to Early Cambrian age (Stöcklin, 1968; Seger, 1977; Berberian and King, 1981). The Kahar Formation is the oldest in the area and consists of diamictites containing detrital zircon that have been dated at ca. 560–550 Ma (Etemad-Saeed et al., 2015; Hassanzadeh et al., 2008).

The late Neoproterozoic to Early Cambrian strata are overlain, with gradational contact, by siliciclastic rocks of the Mila Formation of Middle Cambrian to Ordovician age (Alavi, 1996), subsequently overlain by shales and sandstones of the Ordovician Qelli Formation (Ghavidel-syooki and Winchester-Seeto, 2002). These sedimentary rocks are overlain by voluminous mafic volcanic rocks of the Soltan-Meidan Formation of Late Ordovician to Silurian age (Fig. 2A). The basalt to basaltic-andesite rocks, with transitional to mildly alkaline nature,

mark the continental rift related to the opening of the Paleotethys (e.g., Berberian and King, 1981; Stampfli et al., 1991; Derakhshi et al., 2017). From the Devonian to Late Triassic, thick carbonate and siliciclastic rocks were deposited. In ascending order, they include the Lower to Middle Devonian Padeha sandstones, the Middle to Late Devonian Khosh-Yeilagh sandstones, shales and limestones, and Carboniferous Mobarak Formation of limestones, dolostones and shales (Fig. 2A). Subsequently, Early Permian shales, sandstones and sandy limestones of the Dorud Formation were overlain by micritic limestones of the Ruteh Formation (Fig. 2A). The Dorud Formation of the latest Carboniferous to the Early Permian is composed of shallow-water carbonate shelf sediments, whereas the Ruteh Limestone is considered to represent a wide carbonate ramp deposit (Gaetani et al., 2009). The upper part of the sequence consists of shales and micritic limestones of the Nessen Formation, which was overlain by Early to Middle Triassic carbonate strata of the Elika Formation (Assereto, 1966). In the eastern Alborz Mountains, the Nessen Formation is largely missing and the Geshlagh Formation of arenite and siltstone occur (Jenny and Stampfli, 1978; Gaetani et al., 2009). This unit hosts several lateritic bauxite horizons.

The area was uplifted to subaerial conditions during its collision with Eurasia (Wilmsen et al., 2009), resulting in the formation of fluvial siliciclastic rocks of the Shemshak Formation (Stampfli, 1978; Alavi, 1996) during the Late Triassic to Middle Jurassic period (Seyed-Emami et al., 2006).

### 2.3. Geology of the study area

The oldest exposed rocks in the area close to the Geshlagh deposit are Silurian basalts of the Soltan-Meidan Formation (Fig. 2A). They are overlain by the Devonian Khosh-Yeilagh Formation of fossiliferous limestones and shales, and unconformably by Carboniferous limestones, dolostones and shales of the Mobarak Formation (Fig. 2A). The Early Permian Dorud Formation consists of red to brown sandstones, shales and oncolitic limestones overlain by medium to thick-bedded limestones of the Ruteh Formation (Jafarian and Jalali, 2004; Gaetani et al., 2009). The top of the Ruteh Formation is karstified, and overlain by the Geshlagh Formation, which hosts the Geshlagh bauxite deposit.

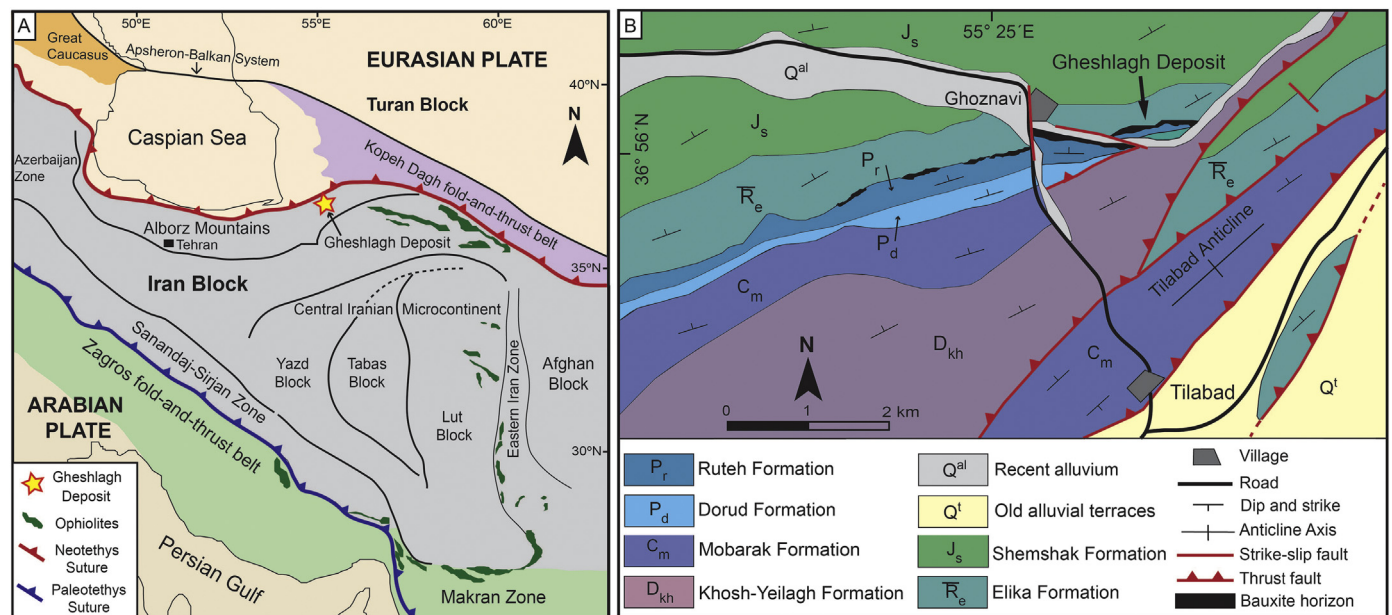


**Fig. 1.** (A) Tectonic framework of Iran and adjacent regions; Neotethys and Paleotethys sutures are indicated (modified after Robert et al., 2014). The Geshlagh deposit (yellow star) is 520 km northeast of Tehran. (B) Simplified geological map of the Geshlagh bauxite deposit in the eastern Alborz Mountains (modified after Jafarian and Jalali, 2004). (For interpretation of the references to colour in this figure legend, the reader is referred to the web version of this article.)

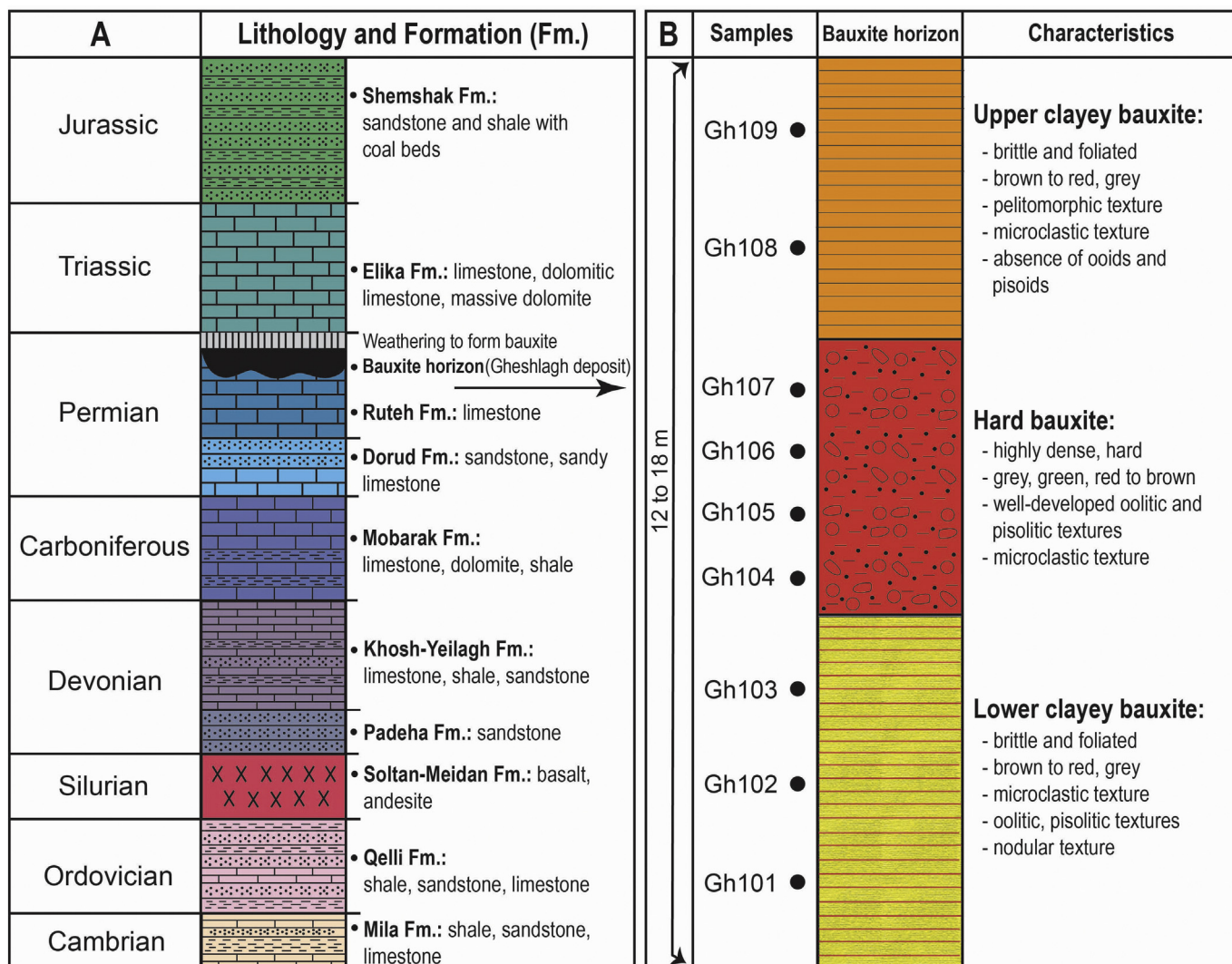


**Fig. 2.** (A) Schematic stratigraphy of the Geshlagh bauxite deposit in the eastern Alborz Mountains (compiled from Assereto, 1966; Alavi, 1996; Seyed-Emami et al., 2006; Fürsich et al., 2009; Wilmsen et al., 2009); thicknesses are not to scale. (B) Schematic columnar section of the Geshlagh bauxite horizon. Sample locations shown by solid circles.

The overlying Early to Middle Triassic Elika Formation (Assereto, 1966; Altiner et al., 1979) consists of thin-bedded vermiculate limestones in the lower part, light green marls with intercalations of thin-bedded dolomitic limestones in the middle part and grayish thick-bedded dolomites to massive dolomites in the upper part (Jafarian and Jalali, 2004; Zamanian Pedram and Karimi, 2007). The Elika Formation is unconformably overlain by alternating sandstone and shale of the Late Triassic to Early Jurassic Shemshak Formation.

The Geshlagh deposit consists of a bauxite horizon with thickness of 12–18 m and strike length of >4 km, unconformably covered by Early Triassic limestone (Figs. 3A, B). Since the bauxite bed overlies a karst, it is classified as a karst-type deposit by Faramarzi et al. (2013) following the classification of Bárdossy (1982). Although there is no evidence for regional metamorphism other than diagenesis, the entire area was deformed, with NE-SW-trending folds, then cut by several reverse and strike-slip faults (Fig. 1B). As a result, exposure of the bauxite bed at the surface is discontinuous along its strike length (Fig. 1B). The bauxite bed has an undulating base (Fig. 3C) and a sharp contact with the overlying limestones (Fig. 3D).

The Geshlagh bauxite deposit is divided into three layers (Fig. 2B): lower clayey bauxite (LCB), hard bauxite (HB) and upper clayey bauxite

(UCB). The red to brown LCB, about 5–8 m in thickness, has abundant nodular concretions (Fig. 3E), and overlies the limestone of the Ruteh Formation. It is mainly composed of hematite, kaolinite, and quartz with lesser rutile and minor diasporite. The green to red layer of HB (Fig. 3F) is about 3–4 m thick and largely composed of diasporite, boehmite, kaolinite, Ti-oxide mineral and hematite. This unit represents the high-grade bauxite ore. The grey to brown layer of UCB is about 4–6 m thick and mainly consists of kaolinite, hematite, and rutile with minor diasporite and Sr-rich aluminum-phosphate-sulphate (APS) minerals.

### 3. Sampling and analytical techniques

#### 3.1. Sampling

During the field work in mid 2017 a total of 52 samples were collected along two sections, from the carbonate footwall to the top of the bauxite layers. A composite sample of bauxite, weighing ~3 kg, was made from five representative samples from HB (Gh107, Gh124, Gh126 and Gh129) and UCB (Gh108) for detrital zircon separation.

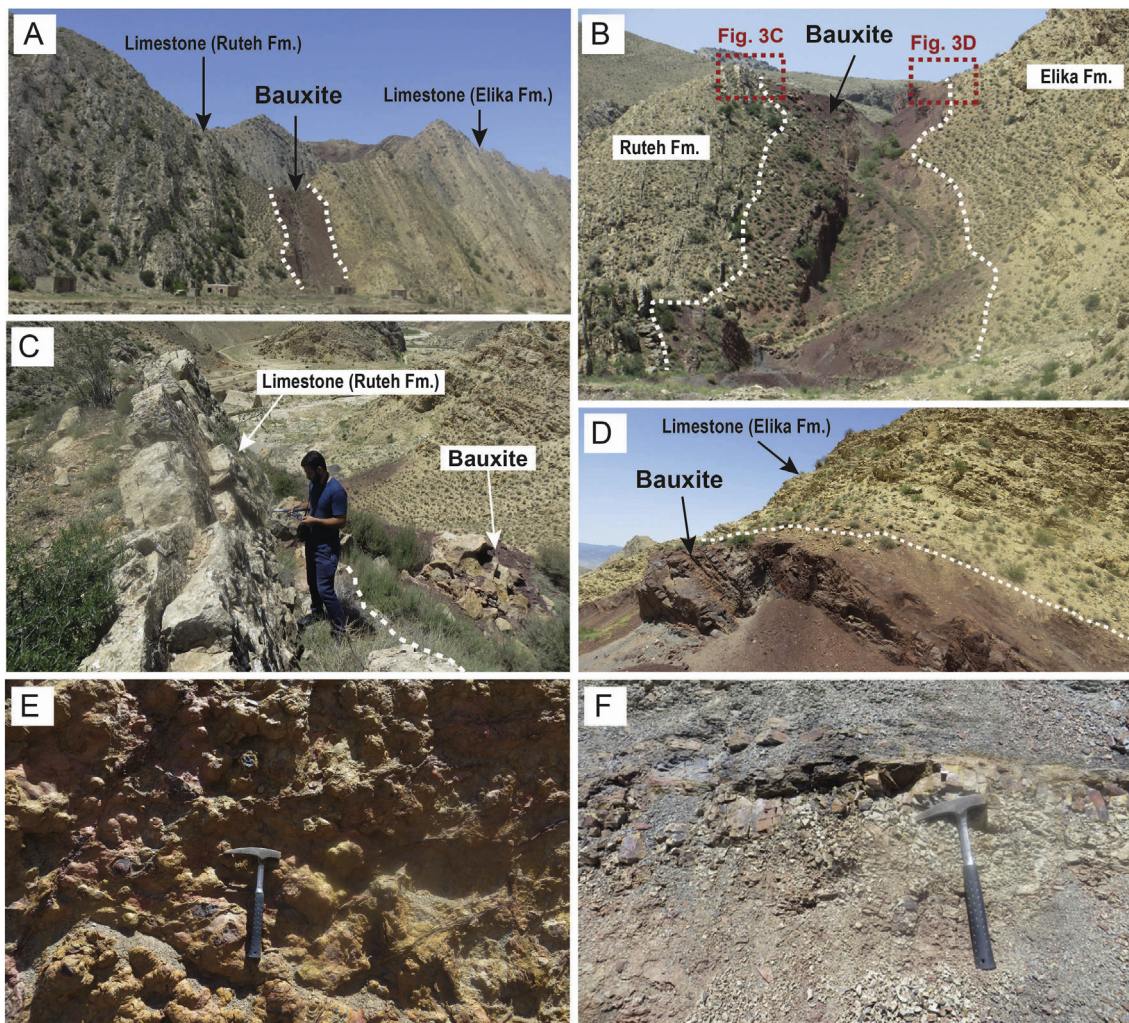


**Fig. 3.** Geshlagh deposit. (A) General view of the Permian limestones, bauxite bed and the Triassic limestones. (B) Mined-out lenticular ore body. (C) Paleokarstic footwall of the ore body. (D) Triassic limestone overlying ore body. (E) Nodular texture of the lower clayey bauxite. (F) Green to red hard bauxite overlying the lower clayey bauxite. (For interpretation of the references to colour in this figure legend, the reader is referred to the web version of this article.)

### 3.2. Mineralogical analyses

The texture and mineralogy of samples were examined using a petrographic microscope, and scanning electron microscopy with energy dispersive spectrometer (SEM-EDS). The mineralogy of nine representative samples (Gh101–109) was determined using a Philips PW 1800 X-ray powder diffractometer at Kansaran Binaloud Research Company, Pardis Science and Technology Park, Tehran. The XRD pattern was recorded over a  $2\theta$  range between 4 and  $70^\circ$ , with counting time of 1 s per  $0.02^\circ$ . Back-scattered electron (BSE) and cathodoluminescence (SEM-CL) images were obtained using a JEOL JSM-6610LV scanning electron microscope in the Department of Earth and Environmental Sciences, University of Ottawa.

### 3.3. Zircon U-Pb dating

The sample was crushed and separated into three size fractions using sieves: 70 # (212  $\mu\text{m}$ ), 120 # (125  $\mu\text{m}$ ), 200 # (75  $\mu\text{m}$ ), and 270 # (53  $\mu\text{m}$ ). Zircon grains were hand-picked under a binocular microscope from heavy mineral fractions, and mounted in epoxy resin. After polishing the epoxy puck to expose the center of grains, zircon grains were examined using a transmitted-light microscope and with BSE and SEM-CL images. Grains without fractures and inclusions were selected for U-Pb dating.

The U-Pb dating were performed with a Photon Machines Analyte Excite 193 nm laser system attached to an Agilent 7700 $\times$  ICP-MS in the Department of Earth and Environmental Sciences, University of Ottawa. The laser was focused to 32  $\mu\text{m}$  in diameter with a repetition rate of 10 Hz. 91,500 zircon and Plešovice zircon were analyzed every seven sample analyses, and used as primary and secondary reference, respectively. A total of 52 areas on 47 detrital zircon grains were analyzed. Raw data were processed using the GLITTER software package (Griffin et al., 2008). A concordia diagram and weighted mean calculations were made with Isoplot/Ex ver. 3.75 (Ludwig, 2012) using a  $^{238}\text{U}/^{235}\text{U}$  ratio of  $137.818 \pm 0.045$ , as defined by Hiess et al. (2012). The analytical procedure is essentially the same as that described by Kobylinski et al. (2020). This paper uses  $^{206}\text{Pb}/^{238}\text{U}$  ages for grains younger than 1000 Ma and  $^{207}\text{Pb}/^{206}\text{Pb}$  ages for older grains (e.g., Compston et al., 1992; Horton et al., 2008; Yu et al., 2016).

## 4. Results

### 4.1. Textures and mineralogy of bauxite

The Geshlagh bauxite ore shows pelitomorphous, microgranular, nodular, clastic, and pisolitic–oolitic textures (Fig. 4). The nodular texture is due to irregular-shaped concretions of variable minerals (Fig. 3E). Ooids, pisoids and rounded to subrounded fragments of

bauxite detrital fragments, mm to cm-sized, comprise the bulk of the bauxite ore (Figs. 4A, B). The pisoids and ooids range from 0.1 to 6 mm in diameter, are spherical to elliptical in shape (Fig. 4C), and consist of thin to thick cortices enclosing single or multiple nuclei of fragments of bauxite (Fig. 4D). Based on XRD analyses, bauxites consist of diaspore (15–30%), boehmite (10–20%), kaolinite (10–60%), hematite (10–40%), rutile (3–10%), and quartz (5–15%), with minor amounts of goethite, chlorite, zircon, and APS minerals.

#### 4.2. Zircon occurrences

Detrital zircons are subhedral (Figs. 5A, B) to anhedral (Figs. 5C, D) and occur in a pelitomorphitic to granular matrix of the bauxite samples. Zircon grains display various shapes that are grouped into four categories (Figs. 6A, B; Table 1). Group I zircons have a needle-like to prismatic crystal shape with elongation (width/length ratio)  $\leq 0.30$ , and sharp oscillatory zoning. Group II zircon grains have a tabular to rounded with elongation from 0.38 to 0.50, and sharp oscillatory zoning (Table 1). The sharp oscillatory zoning in Groups I and II (Figs. 7A, E, K) suggests a magmatic origin of the zircon (Rubatto, 2002; Wang et al., 2016), consistent with their high Th/U ratios, ranging from 0.15 to 1.28 (Table 2). Group III zircon grains are mostly rounded, with elongation 0.51 to 0.68 and variable internal textures, from sharp oscillatory zoning to poorly defined zoning. Group IV represents stubby rounded crystals with elongation  $\geq 0.7$  (Fig. 6B). Some of the rounded grains of Group IV were fragmented, as demonstrated by truncated growth zoning due to erosion (Fig. 8C), suggesting long-distance transportation from the source and/or multiple sedimentary cycles. Zircon grains showing poor zoning of Group III and Group IV have low to intermediate Th/U ratios, 0.04 to 0.43 (Table 1). These grains most likely formed in igneous rocks were affected by sub-solidus alteration during metamorphism or hydrothermal activity, as documented by Corfu et al. (2003). A few grains of Group IV have no discernable zoning (Fig. 7J).

Five grains of Group II show inherited cores surrounded by rims with oscillatory zoning (Figs. 7N, O, Q, R). Inherited cores have Th/U  $> 0.2$ , except for grain Gh-262 (Fig. 7N), which has a ratio 0.12 (Table 2).

#### 4.3. Zircon U-Pb ages

Almost all detrital zircons ( $n = 52$ ) yield concordia ages (Fig. 9), ranging from  $2521 \pm 27.7$  Ma to  $521 \pm 3.6$  Ma, with most ages ( $n = 42$ ) between ca. 975 Ma and 535 Ma. A relative age probability diagram shows dominant peaks at ca. 566 Ma, 641 Ma, 792 Ma, and 847 Ma (Fig. 10). Zircon grains with late Neoproterozoic to Early Cambrian ages (with peak at ca. 566 Ma) are needle-like to prismatic in shape, suggesting proximal sources. The middle to lower Neoproterozoic aged zircons (with peak at ca. 641 Ma) have a tabular to rounded external shape. Four detrital zircon grains have ages of 1029–1132 Ma, and five zircon grains have ages ranging from 1731 to 2521 Ma; the Paleoproterozoic and Neoproterozoic-age zircons are mainly stubby. One detrital zircon grain has an age of 521 Ma.

Inherited cores of five grains yielded ages between ca. 562 Ma to 957 Ma (Table 2; Fig. 9) and the ages of the overgrowth rims are younger than the cores by 8 m.y. to 243 m.y. ( $\pm 1\sigma$  errors of ca. 3–5 m.y.). One exception is grain Gh-190, where the rim (849 Ma) is older than core by ~190 m.y. The younger age of the core is most likely due to Pb loss from the core through cracks after crystallization of the rim, as such reversed age relationship is reported elsewhere (e.g., Gerdes and Zeh, 2009).

## 5. Discussion

#### 5.1. Source of detrital zircons

Ages of zircon grains are related to the morphology, and internal textures (Table 1). Stubby, rounded zircon grains (Group IV) are mainly Paleoproterozoic and Neoproterozoic in age ( $> 1.8$  Ga). Tabular to rounded crystals (Groups II and III) yielding ca. 1.1–0.6 Ga ages. Needle-like to

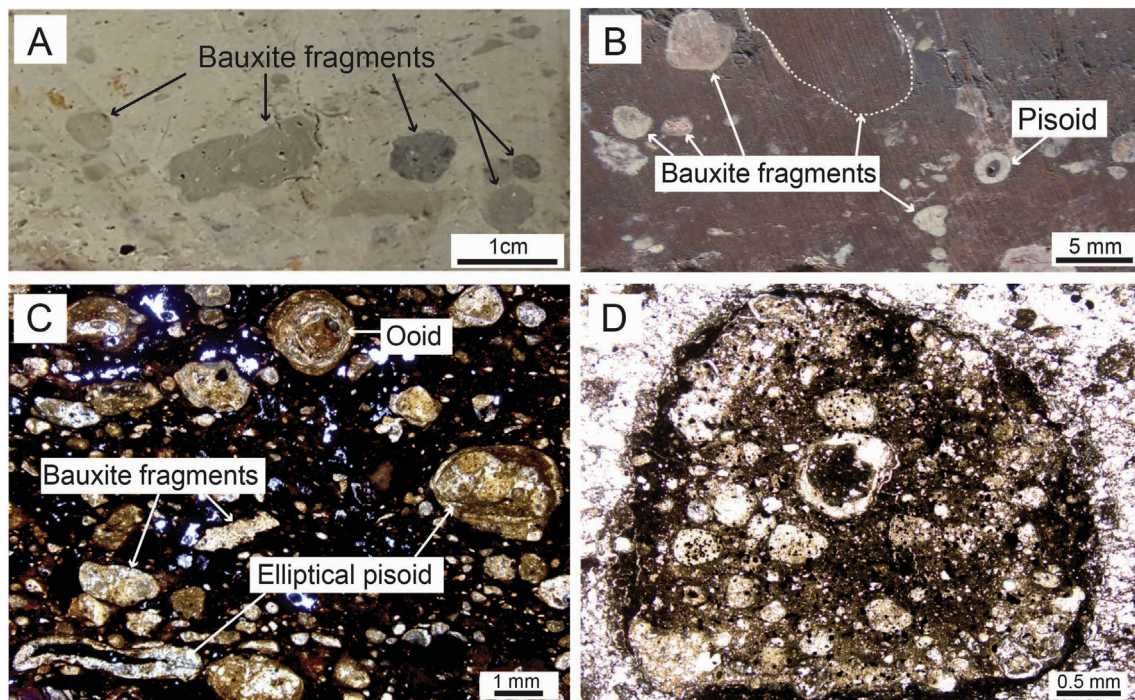


**Fig. 4.** Photographs (A–B) and photomicrographs under polarized transmitted light (C–D) showing the typical textures of bauxite ores from the Geshlagh deposit. (A) Grey to yellow bauxite with clastic texture [sample Gh107]. (B) Red bauxite with pisolitic and oolitic textures [Gh102]. (C) Ferruginous ooids and pisoids of various shapes and sizes [Gh104]. (D) Close-up of complex pisoid with thin cortices enclosing multiple nuclei embedded in a microgranular matrix [Gh106]. (For interpretation of the references to colour in this figure legend, the reader is referred to the web version of this article.)

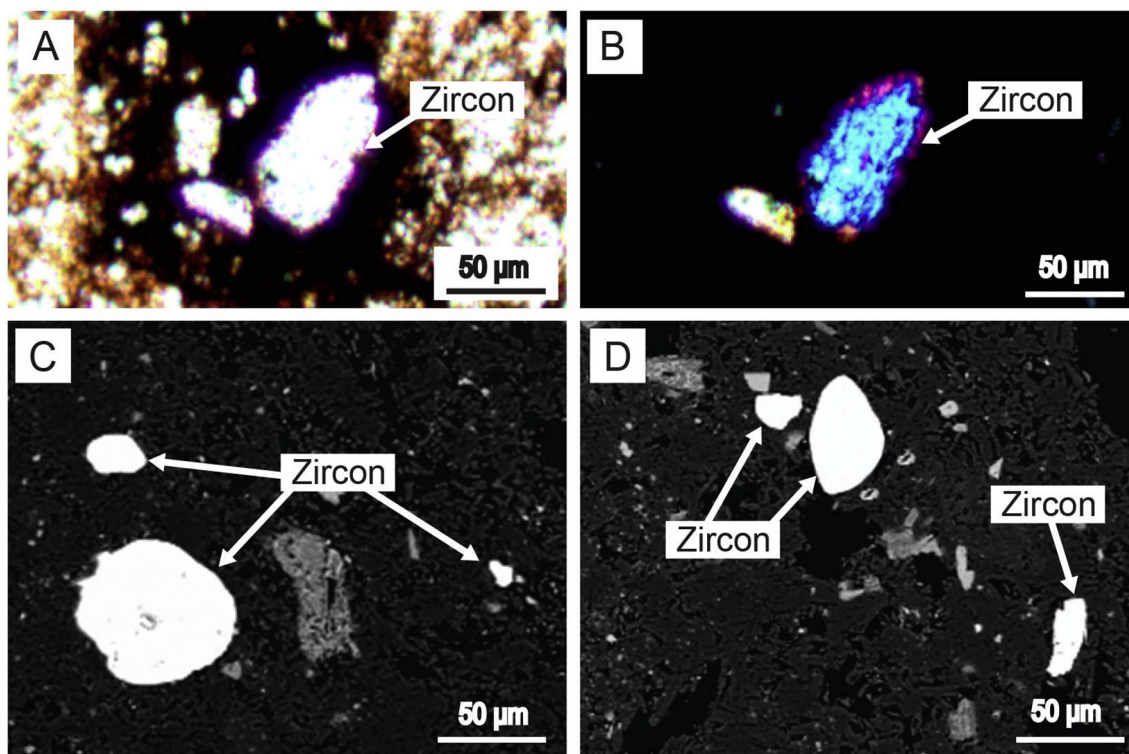


**Fig. 5.** Photomicrograph and BSE images of zircon grains in bauxite ore from the Gheslugh deposit. (A) Zircon grain under plane polarized light and (B) under cross-polarized light [sample Gh108]. (C) BSE image showing the detrital zircon grains of different size in bauxite ore [Ch129]. (D) BSE image of detrital zircons in bauxite ore with pelitomorphic texture [Gh108].

prismatic zircons (Group I) give late Neoproterozoic–Early Cambrian ages (ca. 0.6–0.5 Ga). Zircon grains with sharp oscillatory growth zoning are most likely derived from igneous rocks, whereas zircons with blurred internal zoning likely originated from rocks that have been metamorphosed or hydrothermally altered. The igneous rocks may have been eroded over time, and the evidence for the igneous rocks may be only now be recorded in sedimentary rocks (e.g., Legault and Hattori, 1994; Be’eri-Shlevin et al., 2012). Therefore, the source and provenance of detrital zircon obtained from the Gheslugh bauxite deposit are considered by comparing the ages with those of igneous rocks as well as sedimentary rocks in the region to evaluate possible provenances.

#### 5.1.1. Provenance of detrital zircons older than 1.8 Ga (Group IV)

Zircon grains yielding the ages of ca. 2.5–1.8 Ga are rounded and show blurred oscillatory zoning (Fig. 7, Table 1), suggesting their derivation from distant sources affected by metamorphism. The location of the provenance is not certain, but there are several metamorphic terranes of Archean to Protoproterozoic age in Gondwana, including the Saharan Metacraton in the Arabian-Nubian Shield (ANS) (Abdelsalam et al., 2002). The Kabul Block in the eastern Afghan Central Block is also a possibility, if the block was connected to Gondwana in early Paleozoic time (Faryad et al., 2016; Domeier and Torsvik, 2019) (Fig. 11).

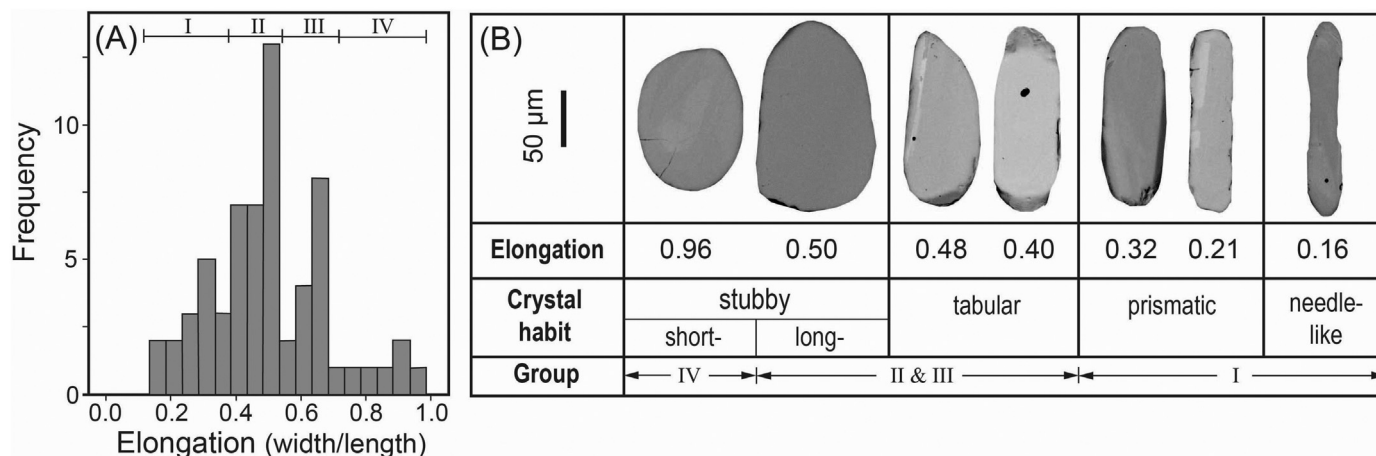


**Fig. 6.** Elongation (width/length ratio) of detrital zircons from the Gheslugh bauxite deposit. (A) Histograms of elongation of detrital zircons showing four groups (I, II, III, and IV) of zircon grains. (B) Various crystal habits of detrital zircons (Group I = needle-like to prismatic, Groups II and III = tabular to rounded external shape, Group IV = stubby). The typology of grains was assessed using the method of Dill (2007) and Gärtner et al. (2013).

**Table 1**

The relationship between morphology, internal texture and U-Pb ages of different detrital zircon groups from the Gheslugh deposit, plus the interpreted provenances.

Morphology <sup>a</sup>	Number of zircon grains	Internal texture	Inherited cores	Th/U	U-Pb ages	Interpreted provenance
Group I (Needle-like to prismatic)	11	Sharp oscillatory zoning	Absent	0.22–0.82	ca. 0.6–0.5 Ga	Cadomian igneous rocks on the northern margin of Gondwana
Group II (Tabular to rounded)	27	Sharp oscillatory zoning	Several grains	0.15–1.28 > 0.2 for core	ca. 0.9–0.6 Ga	Igneous rocks on the Arabian-Nubian Shield
Group III (Mostly rounded)	4	Sharp to poorly oscillatory zoning	Absent	0.30–0.43	ca. 1.1–1 Ga	Metamorphosed/altered Stenian arc igneous rocks
Group IV (Stubby)	5	Blurred zoning	Not clear	0.04–0.30	ca. 2.5–1.8 Ga	Unknown, distant metamorphosed terranes

<sup>a</sup> Morphology shown in Fig. 6.**Fig. 7.** Representative CL images of detrital zircons from the Gheslugh bauxite deposit. Circles indicate the location of laser spots for LA-ICP-MS analysis (using 32 μm laser beam).

**Table 2**  
U–Pb ages of detrital zircons from the Gheshlagh bauxite deposit.

Grain #	Th/U	Isotope ratio						Age (Ma)					
		$^{207}\text{Pb}/^{206}\text{Pb}$	$\pm 1\sigma$	$^{206}\text{Pb}/^{238}\text{U}$	$\pm 1\sigma$	$^{207}\text{Pb}/^{235}\text{U}$	$\pm 1\sigma$	$^{207}\text{Pb}/^{206}\text{Pb}$	$\pm 1\sigma$	$^{206}\text{Pb}/^{238}\text{U}$	$\pm 1\sigma$	$^{207}\text{Pb}/^{235}\text{U}$	$\pm 1\sigma$
Gh-1	0.32	0.07371	0.00137	0.16333	0.00083	1.66004	0.02995	1033	37.1	975	4.6	993	11.4
Gh-2	0.26	0.06022	0.00062	0.10081	0.00027	0.83713	0.00832	611	21.9	619	1.6	618	4.6
Gh-7	0.30	0.10926	0.00092	0.30757	0.00076	4.63431	0.03777	1787	15.3	1729	3.8	1756	6.8
Gh-11	1.28	0.0601	0.00075	0.09158	0.00029	0.75904	0.00925	607	26.9	565	1.7	574	5.3
Gh-14	0.51	0.07031	0.00067	0.1686	0.00044	1.63458	0.01509	937	19.4	1004	2.4	984	5.8
Gh-22	0.29	0.07117	0.00165	0.15748	0.00096	1.54546	0.03484	962	46.6	943	5.3	949	13.9
Gh-29	0.58	0.05956	0.00093	0.10925	0.00043	0.89734	0.01368	588	33.6	668	2.5	650	7.3
Gh-30	0.32	0.06009	0.00113	0.1046	0.00048	0.86681	0.01583	607	40.1	641	2.8	634	8.6
Gh-35	0.30	0.05917	0.00127	0.10413	0.00054	0.84962	0.0178	573	46.1	639	3.1	624	9.8
Gh-43	0.61	0.06439	0.00074	0.13054	0.0004	1.15906	0.0129	754	24.1	791	2.3	782	6.1
Gh-49	0.66	0.07041	0.00079	0.15499	0.00047	1.50485	0.01631	940	22.7	929	2.7	932	6.6
Gh-55	0.63	0.06807	0.00147	0.13828	0.00077	1.29799	0.02728	871	44.1	835	4.4	845	12.1
Gh-68	0.33	0.05874	0.00084	0.10476	0.00038	0.84848	0.01178	557	30.8	642	2.2	624	6.5
Gh-93	0.52	0.06106	0.00146	0.10197	0.00059	0.85865	0.02006	641	50.7	626	3.4	629	11.0
Gh-95	0.45	0.06627	0.00084	0.13975	0.00047	1.27714	0.01569	815	26.2	843	2.7	836	7.0
Gh-96	0.37	0.10594	0.00098	0.24661	0.00066	3.60265	0.0323	1731	16.9	1421	3.4	1550	7.1
Gh-105	0.22	0.05857	0.00081	0.1027	0.00036	0.82954	0.01112	551	29.8	630	2.1	613	6.2
Gh-109	0.79	0.05797	0.00085	0.08872	0.00033	0.70923	0.01008	528	32.1	548	2.0	544	6.0
Gh-113	0.43	0.06904	0.00204	0.12957	0.00099	1.23348	0.03543	899	59.7	785	5.6	816	16.1
Gh-118	0.58	0.0551	0.00301	0.08649	0.00091	0.65717	0.03537	416	117.4	535	5.4	513	21.7
Gh-121	0.30	0.05654	0.00112	0.09194	0.00044	0.71688	0.01386	473	43.7	567	2.6	549	8.2
Gh-124	0.32	0.07073	0.00107	0.16427	0.00069	1.60223	0.02354	949	30.7	981	3.8	971	9.2
Gh-129	0.35	0.07439	0.00079	0.18056	0.00053	1.85226	0.01898	1052	21.2	1070	2.9	1064	6.8
Gh-136	0.51	0.06689	0.00143	0.15467	0.00086	1.42672	0.02975	834	44.1	927	4.8	900	12.5
Gh-146	0.35	0.15482	0.00163	0.45748	0.00151	9.76738	0.09918	2400	17.8	2429	6.7	2413	9.4
Gh-159	0.49	0.06795	0.00095	0.15302	0.00058	1.43382	0.01939	867	28.7	918	3.2	903	8.1
Gh-172	0.90	0.06359	0.00119	0.13105	0.00063	1.1492	0.02093	728	39.2	794	3.6	777	9.9
Gh-173	0.43	0.07741	0.00164	0.17127	0.00102	1.82847	0.03754	1132	41.7	1019	5.6	1056	13.5
Gh-174	0.52	0.06493	0.0013	0.12162	0.00063	1.08906	0.02127	772	41.7	740	3.6	748	10.3
Gh-177	0.68	0.06086	0.00163	0.10308	0.00069	0.86511	0.02259	634	56.8	632	4.0	633	12.3
Gh-188 C	0.54	0.06626	0.00211	0.09109	0.00069	0.83233	0.02583	814	65.1	562	4.1	615	14.3
Gh-188 R	0.82	0.05971	0.0016	0.08865	0.00056	0.73003	0.01906	593	56.7	548	3.3	557	11.2
Gh-190 C	0.23	0.06399	0.00094	0.10754	0.00042	0.94898	0.01351	741	30.8	659	2.4	678	7.0
Gh-190 R	0.57	0.06813	0.00092	0.14081	0.00051	1.32291	0.01722	872	27.6	849	2.9	856	7.5
Gh-201	0.30	0.07355	0.00125	0.17083	0.0008	1.73277	0.0285	1029	33.9	1017	4.4	1021	10.6
Gh-209	0.79	0.05779	0.00181	0.08423	0.0006	0.67138	0.02059	522	67.6	521	3.6	522	12.5
Gh-213	0.33	0.10805	0.00172	0.28979	0.00138	4.3178	0.06596	1767	28.8	1641	6.9	1697	12.6
Gh-214 C	0.83	0.05665	0.00131	0.09258	0.00052	0.72327	0.01621	641	98.1	571	3.1	553	9.6
Gh-214 R	1.12	0.06106	0.00287	0.09102	0.00094	0.76642	0.03529	477	50.5	562	5.5	578	20.3
Gh-215	0.04	0.16634	0.00277	0.48705	0.00306	11.17268	0.17864	2521	27.7	2558	13.3	2538	14.9
Gh-226	0.64	0.06152	0.00199	0.09615	0.00072	0.8158	0.02572	658	67.8	592	4.2	606	14.4
Gh-232	0.47	0.06696	0.00106	0.14044	0.0006	1.29694	0.01982	837	32.7	847	3.4	844	8.8
Gh-233	0.19	0.0716	0.00132	0.18645	0.00094	1.84111	0.03277	975	37.1	1102	5.1	1060	11.7
Gh-238 C	0.68	0.05954	0.00117	0.09782	0.00049	0.80321	0.01538	593	43.4	602	2.9	599	8.7
Gh-238 R	0.32	0.05971	0.00122	0.09645	0.00049	0.79419	0.01579	587	42.2	594	2.9	594	8.9
Gh-241	0.41	0.06993	0.00225	0.15665	0.00128	1.51065	0.04737	926	64.8	938	7.2	935	19.2
Gh-242	0.15	0.06583	0.00228	0.12273	0.00101	1.11421	0.03772	801	71.1	746	5.8	760	18.1
Gh-250	0.42	0.06362	0.00141	0.12958	0.00073	1.13685	0.02446	730	46.3	785	4.2	771	11.6
Gh-260	0.60	0.06898	0.0015	0.13734	0.0008	1.30641	0.02752	899	44.3	830	4.6	849	12.1
Gh-261	0.38	0.07085	0.00117	0.15213	0.00068	1.48641	0.02367	953	33.3	913	3.8	925	9.7
Gh-262 C	0.12	0.06973	0.00115	0.16006	0.00072	1.53931	0.02464	921	33.7	957	4.0	946	9.9
Gh-262 R	0.40	0.06366	0.00109	0.11716	0.00052	1.02864	0.01698	730	35.7	714	3.0	718	8.5

Uncertainties of individual analyses are presented as  $1\sigma$ . C and R refer to core and rim of zircon grain.

### 5.1.2. Provenance of detrital zircons with ages around 1 Ga (Group III)

Detrital zircons from the Gheshlagh deposit with ages of ca. 1.1–1 Ga have a rounded shape (Group III of Table 1) suggesting a long distance transport or multiple sedimentary cycles. Oscillatory zoning is clear in some grains, but blurred in other grains. There are several possible provenances for these zircon grains. They include Sinai basement rocks in the northernmost part of the ANS (Fig. 11), where metamorphosed igneous rocks of the Stenian arc (ca. 1.03–1.02 Ga; Be'eri-Shlevin et al., 2012) are recognized in Sa'al metasedimentary rocks (1.11–1.03 Ga; Be'eri-Shlevin et al., 2009). Since the detrital zircon grains derived from Stenian igneous rocks are also common in Early Paleozoic sandstones in northern Africa (Meinhold et al., 2013), the erosion of these sedimentary rocks might have provided zircon grains to the Gheshlagh deposit.

### 5.1.3. Provenance of detrital zircons with ages between 1 and 0.6 Ga (Group II)

U–Pb ages of detrital zircons from the Gheshlagh deposit between ca. 0.9 and 0.6 Ga in age (Group II of Table 1) show sharp oscillatory growth zoning (Figs. 7E, K). The age spectra are similar to those of detrital zircons from late Neoproterozoic–Cambrian sedimentary rocks in many locations in the ANS reported by Johnson (2014) (Fig. 12). These include the Rutig conglomerate and Elat conglomerate in the northern part of the ANS (Fig. 12A), the Abt Formation in the eastern part of the shield (Fig. 12B), and the sedimentary rocks of the Huqf Supergroup, and Cambro-Ordovician sandstones on the northern margin of the shield (Fig. 12C). These detrital zircon grains are considered to have been sourced from proximal igneous rocks, based on morphology and internal textures (Kolodner et al., 2006).

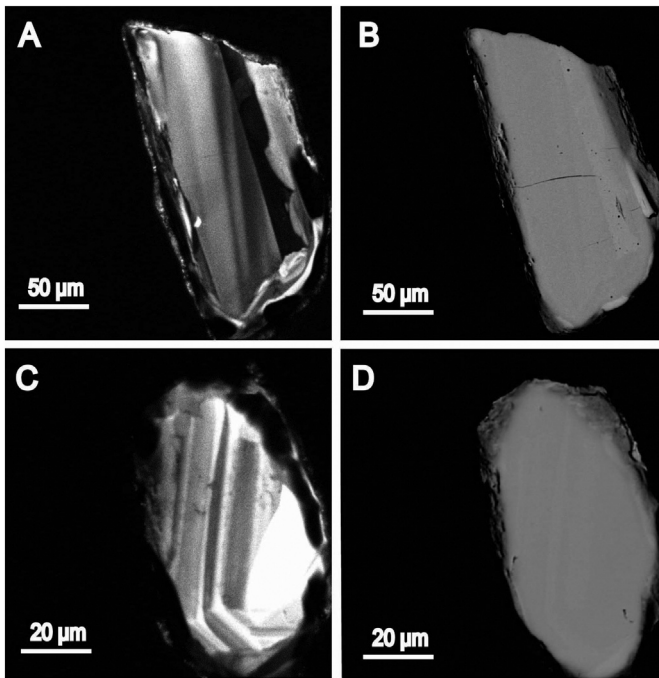


**Fig. 8.** Broken faces of detrital zircons from the Geshlagh deposit. (A) Cathodoluminescence (CL) and (B) BSE images showing broken detrital zircon [sample Gh-159]. (C) CL and (D) BSE images of fragmented detrital zircon grain showing oscillatory zoning in the interior of the zircon [sample Gh-173].

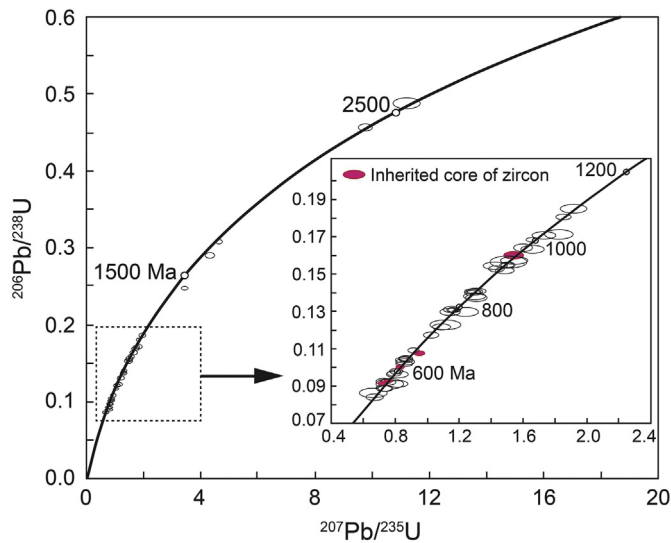


**Fig. 9.** U-Pb concordia diagram of detrital zircons from the Geshlagh bauxite deposit.

Detrital zircons in the Geshlagh deposit show a population peak at 641 Ma, which is also observed in the above mentioned sedimentary rocks of the ANS (Fig. 12). Granitic rocks associated with the East African Orogeny are abundant in the northern ANS (Fig. 11), with U-Pb zircon ages of  $637 \pm 5$  (Ali et al., 2010, 2012). Zircon grains with older age populations, ranging from ca. 714 Ma to 938 Ma with two major peaks at 792 Ma and 847 Ma, may have originated from igneous rocks of the Tonian–Cryogenian arc in the northern (Morag et al., 2011) and eastern parts of ANS (Stern, 2002; Stern and Johnson, 2010). These subduction-related igneous rocks range in age from ca. 870 to 630 Ma (Stern and Johnson, 2010).

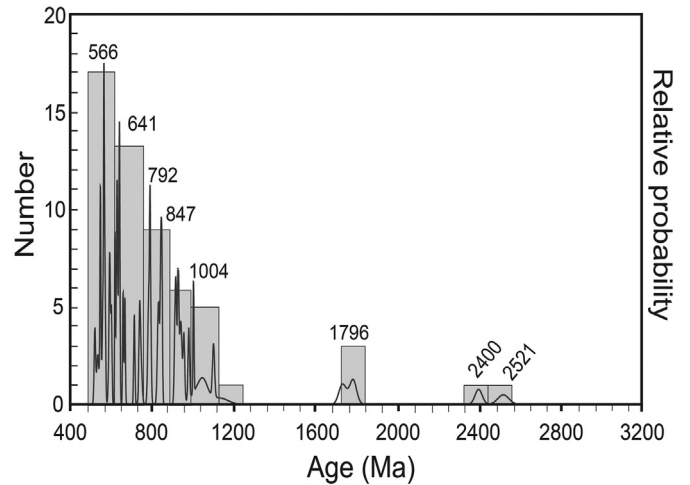


**Fig. 10.** Relative age probability diagram displaying the U-Pb detrital zircon age distribution for the Geshlagh bauxite deposit.

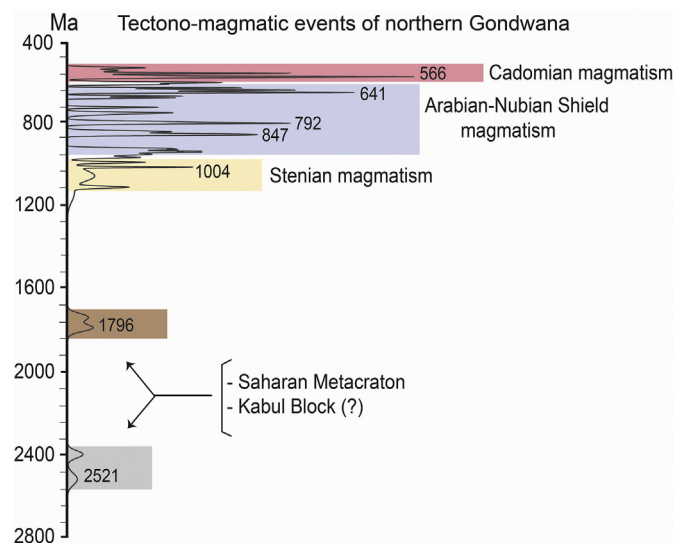


**Fig. 11.** Detrital zircon age spectrum of the Geshlagh bauxite deposit versus the tectono-magmatic events of northern Gondwana.

5.1.4. Source of zircon grains younger than 600 Ma (Group I)

The Geshlagh deposit contains zircon grains younger than 600 Ma, with a population peak at ~566 Ma and the youngest age of 521 Ma (Fig. 10). They were supplied from proximal igneous rocks based on their delicate needle-like shape and sharp oscillatory zoning (Table 1). We suggest that they likely derived from Cadomian arc rocks (600–500 Ma), which formed on the northern margin of Gondwana due to southward subduction of Prototethys (Ustaömer et al., 2009; Garfunkel, 2015) from ~600 Ma for 100 m.y. (Moghadam et al., 2017a; Fig. 13A). The youngest age of zircon, 521 Ma, from the Geshlagh deposit suggests that Cadomian magmatic activity likely continued in the region to the Early Cambrian.

The proposed interpretation is further supported by the occurrence of Cadomian igneous zircon as detrital grains in early Paleozoic sedimentary rocks of the Alborz Mountains, reported by Horton et al. (2008) and Moghadam et al. (2017b) (Figs. 12D, E). The data suggest the paleo current was such that Cadomian arc rocks on the northern margin of the ANS provided detritus to the area.

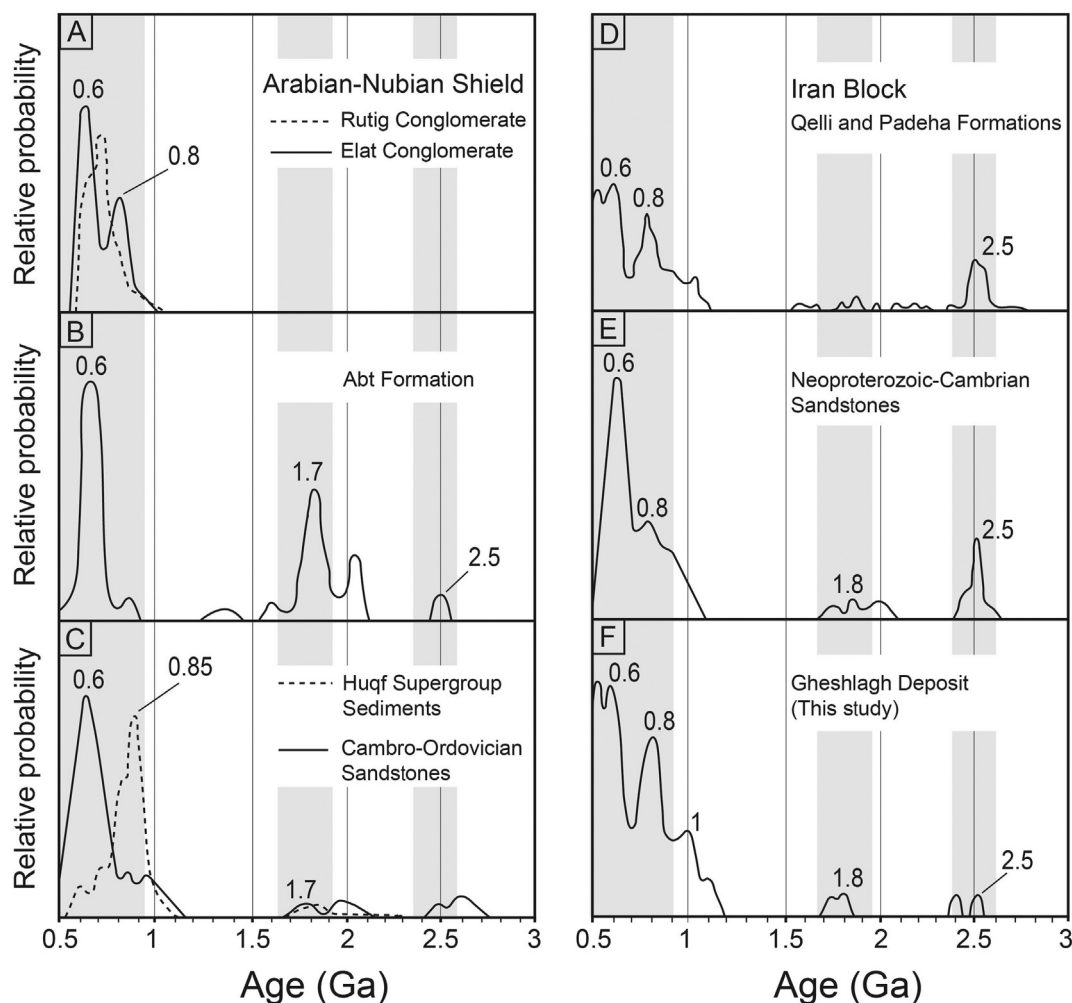


**Fig. 12.** Relative probability plots for U-Pb ages of detrital zircons from sedimentary rocks in the Iran Block and the ANS. (A) Rutig and Elat Conglomerates in the northern ANS; (B) Abt Formation in the eastern ANS; (C) Huqf Supergroup sedimentary rocks and Cambro-Ordovician sandstones on the northern margin of the ANS; (D) Qelli and Padeha Formations in north-eastern Iran Block; (E) Neoproterozoic-Cambrian sandstones in the Iran Block; (F) Geshlagh deposit in northern Iran (this study). Data sources for A, B, C are Johnson (2014), and for D, E from Horton et al. (2008) and Moghadam et al. (2017b).

### 5.2. History of the Cimmerian terrane: evidence from bauxite deposit

The detrital zircon populations of the Geshlagh deposit are dominated by Neoproterozoic–Early Cambrian ages, especially those between 0.9 and 0.5 Ga, with smaller zircon populations of older ages. The ages ranging from 0.9 to 0.6 Ga and from 0.6 to 0.5 Ga overlap with those of igneous rocks in the interior of ANS and Cadomian arc rocks on the northern margin of ANS, respectively (Table 1). Our new zircon ages suggest that the Cimmerian Continent was still part of Gondwana during the deposition of the bauxite protolith in the Permian. Our proposed interpretation agrees with the paleogeographic reconstruction of the Iran Block by Horton et al. (2008), based on U-Pb ages of detrital zircon from early Paleozoic strata of the Alborz Mountains.

We suggest that the bauxite protolith was deposited on the northern margin of Gondwana where detritus was transported northward from the interior of ANS. After protolith deposition of the Geshlagh deposit in Late Permian time, the Cimmerian Continent rifted from Gondwana very end of Permian (Fig. 13B). There is the evidence for southward subduction of Paleotethys below the northern margin of Gondwana in very late Carboniferous period (e.g., Candan et al., 2016); this rifting of the Cimmerian Continent may have initiated in a back-arc configuration, as has been proposed by Sengör (1987) and Santosh et al. (2009).

Incorporation of detrital zircons in sediments requires the exposure and erosion of zircon-bearing rocks in provenances and the transportation of zircon to the depositional sites. Age spectra of detrital zircons from the Geshlagh bauxite deposit suggest that the rocks on the northern part of ANS were the dominant contributors to the detritus of the bauxite deposit. Interestingly, detrital zircon with ages younger than 520 Ma are lacking in the Geshlagh deposit, but zircon grains with ages of 492–404 Ma are reported from Paleozoic siliciclastic rocks of the Alborz Mountains (Moghadam et al., 2017b). The lack of young zircon grains in the Geshlagh deposit may be explained by the paleogeography of the area during deposition of the Geshlagh bauxite protolith in the Permian period. Ordovician–Silurian felsic igneous rocks occur in the northern part of the Iran Block, but their distribution is limited and far from the depositional site. On the other hand, the area proximal to the Geshlagh deposit was covered by voluminous Silurian basaltic rocks, with thickness up to about 1300 m (Derakhshi et al., 2017). These basaltic rocks (with ~184 ppm Zr; Derakhshi et al., 2017) do not contain zircon grains because crystallization of zircon requires more than 1200 ppm Zr in basaltic magmas, based on the Zr saturation equation of Watson and Harrison (1983). More importantly, the voluminous basaltic rocks occur between Ordovician–Silurian felsic rocks and the depositional site. Such thick basaltic rocks likely prevented the supply of zircon from more distant locations.

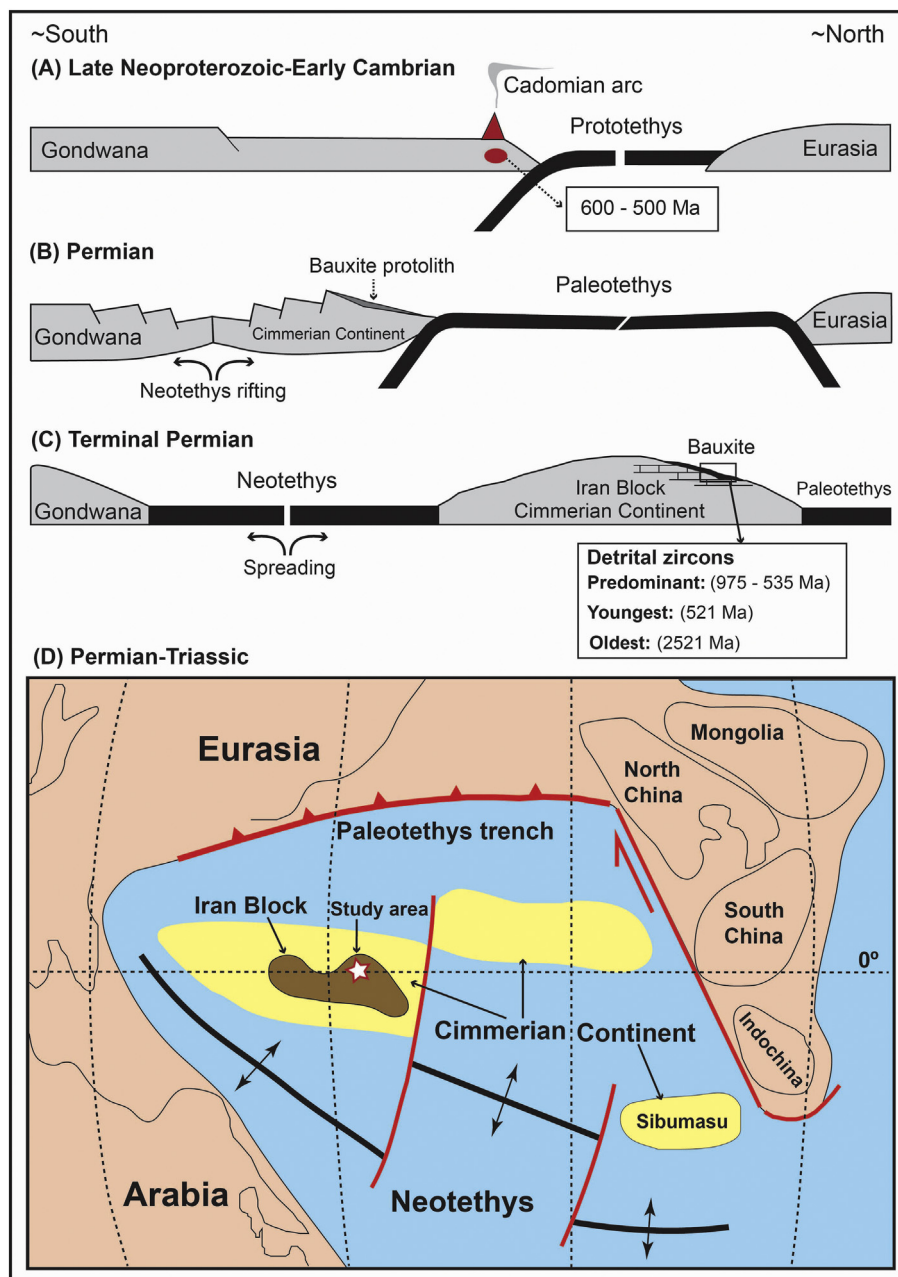


**Fig. 13.** Schematic diagrams showing plate tectonic and paleogeographic evolution of the Cimmerian Continent and Iran Block from late Neoproterozoic to Late Permian, including closure of the Paleotethys. (A) Late Neoproterozoic–Early Cambrian subduction along northern Gondwana. (B) Neotethys rifting of the Cimmerian Continent, including the Iran Block, in the Permian. (C) Northward motion of the Cimmerian Continent during Neotethys opening in the terminal Permian period. (D) Paleogeographic reconstruction of the Iran Block for the Permian–Triassic (modified after Muttoni et al., 2009b). The approximate location of the study area is shown by the white star. Subduction zone = lines with barbs on the upper plate; oceanic ridge = small diverging arrows.

The Cimmerian Continent migrated northward (Fig. 13C), attaining subequatorial paleolatitudes in the Permian–Triassic time (Fig. 13D) (Muttoni et al., 2009b), resulting in a tropical climate conducive to the formation of bauxites and laterites. Due to the fragmentation of the continent, these deposits are now distributed in northern Iran, the Tauride Belt in southern Turkey (Haniççi, 2013), southern and central Afghanistan (Renaud et al., 2015), and Kattha of western Pakistan (Ashraf et al., 1972).

## 6. Conclusions

1) Detrital zircon grains from the Geshlagh bauxite deposit record a principal age population at ~0.9–0.5 Ga with smaller populations at

~1 Ga and ~2.5–1.8 Ga. Zircon morphologies suggest distal sources for zircon grains older than 0.6 Ga and proximal sources for those younger than 0.6 Ga.

- 2) Detrital zircons with ages younger than 0.6 Ga were likely sourced from Cadomian igneous rocks (ca. 0.6–0.5 Ga), on the northern margin of Gondwana. Detrital zircons with ages of ca. 0.9–0.6 Ga most likely originated from igneous rocks in the interior of the ANS. The detrital zircons with ages of ~1 Ga were probably derived from Sinai basement rocks, whereas zircons with ages of ~2.5 Ga have several possible sources, including the Saharan Metacraton and Kabul Block.
- 3) The new U–Pb zircon ages suggest that the Cimmerian terrane was still located on the northern margin of Gondwana during deposition

of the bauxite protolith in the Permian. The equatorial paleolatitudes of the western Cimmerian Continent during the Late Permian allowed intense weathering to form numerous bauxite deposits.

### Declaration of Competing Interest

The authors declare that they have no known competing financial interests or personal relationships that could have appeared to influence the work reported in this paper.

### Acknowledgements

This research was supported by grants from the Deputy of Research and Technology of Golestan University, Iran, to GHS (20607/15-02-2017); Discovery Grant from Natural Sciences and Engineering Research Council of Canada awarded to KH (ORCID 0000-0002-6757-707X). Much of the analytical work was conducted while GHS was a visiting professor at the University of Ottawa. We thank Glenn Poirier for assistance with SEM work, Samuel Morfin for LA-ICP-MS analyses, Martin Viala for zircon data reduction, Alain Mauviel for preparation of polished thin sections, and Richard Goldfarb and Jeffrey Hedenquist for their comments on earlier versions of this manuscript, including idiomatic editing. We are very grateful to two anonymous reviewers for their constructive reviews of the manuscript, which improved the context of our interpretation.

### References

- Abdelsalam, M.G., Liégeois, J.-P., Stern, R.J., 2002. The Saharan metacraton. *J. Afr. Earth Sci.* 34, 119–136.
- Alavi, M., 1996. Tectonostratigraphic synthesis and structural style of the Alborz mountain system in northern Iran. *J. Geodyn.* 21, 1–33.
- Ali, K.A., Stern, R.J., Manton, W.I., Kimura, J.I., Whitehouse, M.J., Mukherjee, S.K., Johnson, P.R., Griffin, W.R., 2010. Geochemical, U–Pb zircon, and Nd isotope investigations of the Neoproterozoic Ghawjah Metavolcanic rocks, Northwestern Saudi Arabia. *Lithos* 120, 379–392.
- Ali, K., Andresen, A., Manton, W.I., Stern, R.J., Omar, S.A., Maurice, A.E., 2012. U–Pb zircon dating and Sr–Nd–Hf isotopic evidence to support a juvenile origin of the ~634 Ma El Shalul granitic gneiss dome, Arabian–Nubian Shield. *Geol. Mag.* 149, 783–797.
- Altiner, D., Baud, A., Guex, J., Stampfli, G., 1979. La limite Permien-Trias dans quelques localités du Moyen-Orient: recherches stratigraphiques et micropaléontologiques. *Riv. Ital. Paleontol. S.* 85, 683–714.
- Angiolini, L., Zanchi, A., Zanchetta, S., Nicora, A., Vuolo, I., Berra, F., Henderson, C., Malaspina, N., Rettori, R., Vachard, D., Vezzoli, G., 2015. From rift to drift in South Pamir (Tajikistan): Permian evolution of a Cimmerian terrane. *J. Afr. Earth Sci.* 102, 146–169.
- Ashraf, M., Chohan, N.A., Faruqi, F.A., 1972. Bauxite and clay deposits in the Kattha Area, Salt Range, Punjab, West Pakistan. *Econ. Geol.* 67, 103–110.
- Assereto, R., 1966. The Jurassic Shemshak Formation in central Elburz (Iran). *Riv. Ital. Paleontol. S.* 72, 1133–1182.
- Bárdossy, G., 1982. Karst Bauxites, Bauxite Deposits on Carbonate Rocks. Elsevier Science and Technology Books, p. 441.
- Bárdossy, G., Aleva, G.J.J., 1990. Lateritic Bauxites. *Development in Economic Geology*. 27. Elsevier, Amsterdam, p. 624.
- Be'eri-Shlevin, Y., Katzir, Y., Whitehouse, M.J., Kleinhanns, C.I., 2009. Contribution of pre Pan-African crust to formation of the Arabian Nubian Shield: New secondary ionization mass spectrometry U–Pb and O studies of zircon. *Geology* 37, 899–902.
- Be'eri-Shlevin, Y., Eyal, M., Eyal, Y., Whitehouse, M.J., Litvinovsky, B., 2012. The Sa'al volcano-sedimentary complex (Sinai, Egypt): A latest Mesoproterozoic volcanic arc in the northern Arabian Nubian Shield. *Geology* 40, 403–406.
- Berberian, M., King, G.C.P., 1981. Towards a palaeogeography and tectonic evolution of Iran. *Can. J. Earth Sci.* 18, 210–265.
- Bogatyrev, B.A., Zhukov, V.V., Tskhovsky, Yu.G., 2009. Formation conditions and regularities of the distribution of large and superlarge bauxite deposits. *Lithol. Miner. Resour.* 44, 135–151.
- Cai, S., Wang, Q., Liu, X., Feng, Y., Zhang, Y., 2015. Petrography and detrital zircon study of late Carboniferous sequences in the southwestern North China Craton: implications for the regional tectonic evolution and bauxite genesis. *J. Asian Earth Sci.* 98, 421–435.
- Candan, O., Akal, C., Koralay, O.E., Okay, A.I., Oberhänsli, R., Prelević, D., Mertz-Kraus, R., 2016. Carboniferous granites on the northern margin of Gondwana, Anatolide-Tauride Block, Turkey – evidence for southward subduction of Paleotethys. *Tectonophysics* 683, 349–366.
- Compston, W., Williams, I., Kirschvink, J., Zichao, Z., Guogan, M., 1992. Zircon U–Pb ages for the Early Cambrian time-scale. *J. Geol. Soc. Lond.* 149, 171–184.
- Corfu, F., Hanchar, J.M., Hoskin, P.W.O., Kinny, P., 2003. Atlas of zircon textures. *Rev. Mineral. Geochem.* 53, 469–500.
- Derakhshi, M., Ghasemi, H., Miao, L., 2017. Geochemistry and petrogenesis of Soltan-Maidan basalts (E Alborz, Iran): Implications for asthenosphere-lithosphere interaction and rifting along the N margin of Gondwana. *Chem. Erde Geochem.* 77, 131–145.
- Dill, H., 2007. Grain morphology of heavy minerals from marine and continental placer deposits, with special reference to Fe–Ti oxides. *Sediment. Geol.* 198, 1–27.
- Domeier, M., Torsvik, T.H., 2019. Full-plate modelling in pre-Jurassic time. *Geol. Mag.* 156, 261–280. <https://doi.org/10.1017/S0016756817001005>.
- Etemad-Saeed, N., Hosseini-Barzi, M., Adabi, M., Miller, N.R., Sadeghi, A., Houshmandzadeh, A., Stockli, D.F., 2015. Evidence for ca. 560 Ma Ediacaran glaciation in the Kahar Formation, central Alborz Mountains, northern Iran. *Gondwana Res.* 31, 164–183.
- Faramarzi, R., Shamanian, G.H., Shafiei, B., 2013. Gheshlagh Permo-Triassic bauxite deposit in the Eastern-Alborz Zone: geology and petrography. *Iran. J. Crystallogr. Mineral.* 21, 71–82 (in Persian with English abstract).
- Faryad, S.W., Collett, S., Finger, F., Sergeev, S.A., Čopjaková, R., Siman, P., 2016. The Kabul Block (Afghanistan), a segment of the Columbia Supercontinent, with a Neoproterozoic metamorphic overprint. *Gondwana Res.* 34, 221–240.
- Fürsich, F.T., Wilmsen, M., Seyed-Emami, K., Majidifard, M.R., 2009. Lithostratigraphy of the Upper Triassic–Middle Jurassic Shemshak Group of northern Iran. In: Brunet, M.F., Wilmsen, M., Granath, J. (Eds.), *South Caspian to Central Iran Basins*. *Geol. Soc. Lond. Spec. Publ.* vol. 312, pp. 129–160.
- Gaetani, M., Angiolini, L., Ueno, K., Nicora, A., Stephenson, M.H., Sciunnach, D., Rettori, R., Price, G.D., Sabouri, J., 2009. Pennsylvanian–Early Triassic stratigraphy in the Alborz Mountains, Iran. In: Brunet, M.F., Wilmsen, M., Granath, J. (Eds.), *South Caspian to Central Iran Basins*. *Geol. Soc. Lond. Spec. Publ.* vol. 312, pp. 129–160.
- Garfunkel, Z., 2015. The relations between Gondwana and the adjacent Peripheral Cadomian Domain—constraints on the origin, history, and paleogeography of the Peripheral Domain. *Gondwana Res.* 28, 1257–1281.
- Gärtner, A., Linnemann, U., Sagawe, A., Hofmann, M., Ullrich, B., Kleber, A., 2013. Morphology of zircon crystal grains in sediments—characteristics, classifications, definitions. *Geol. Saxon.* 59, 65–73.
- Gerdes, A., Zeh, A., 2009. Zircon formation versus zircon alteration—new insights from combined U–Pb and Lu–Hf in-situ LA-ICP-MS analyses, and consequences for the interpretation of Archean zircon from the Central Zone of the Limpopo Belt. *Chem. Geol.* 261, 230–243.
- Ghavidel-Syooki, M., 1995. Palynostratigraphy and palaeogeography of a Palaeozoic sequence in the Hassanakdar area, central Alborz range, northern Iran. *Rev. Palaeobot. Palynol.* 86, 91–109.
- Ghavidel-Syooki, M., 2008. Palynostratigraphy and palaeogeography of the Upper Ordovician Gorgan Schists (Southeastern Caspian Sea), Eastern Alborz Mountain Ranges, Northern Iran. *Commun. Geol.* 95, 123–155.
- Ghavidel-Syooki, M., Winchester-Seeto, T., 2002. Biostratigraphy and palaeogeography of Late Ordovician chitinozoans from the northeastern Alborz Range, Iran. *Rev. Palaeobot. Palynol.* 118, 77–99.
- Griffin, W.L., Powell, W.J., Pearson, N.J., O'Reilly, S.Y., 2008. GLITTER: data reduction software for laser ablation ICP-MS. *Laser ablation-ICP-MS in the Earth sciences*. *Mineral. Assoc. Canada Short Course Ser.* 40, 204–207.
- Haniçi, N., 2013. Geological and geochemical evolution of the Bolkardaği bauxite deposits, Karaman, Turkey: transformation from shale to bauxite. *J. Geochem. Explor.* 133, 118–137.
- Hassanzadeh, J., Stockli, D.F., Horton, B.K., Axen, G.J., Stockli, L.D., Grove, M., Schmitt, A., Walker, J.D., 2008. U–Pb zircon geochronology of upper Neoproterozoic–Early Cambrian granitoids in Iran: implications for palaeogeography, metallogeny, and exhumation history of Iranian basement. *Tectonophysics* 451, 71–96.
- Hieiss, J., Condon, D.J., McLean, N., Noble, S.R., 2012. <sup>238</sup>U/<sup>235</sup>U systematics in terrestrial uranium-bearing minerals. *Science* 335, 1610–1614.
- Horton, B.K., Hassanzadeh, J., Stockli, D.F., Axen, G.J., Gillis, R.J., Guest, B., Amini, A., Fakhari, M.D., Zamanzadeh, S.M., Grove, M., 2008. Detrital zircon provenance of Neoproterozoic to Cenozoic deposits in Iran: implications for chronostratigraphy and collisional tectonics. *Tectonophysics* 451, 97–122.
- Jafarian, M.B., Jalali, A., 2004. Geological Map of Khosh-Yeilagh (Scale 1:100,000). Geological Survey of Iran, Tehran.
- Jenny, J., Stampfli, G., 1978. Lithostratigraphie du Permien de l'Elbourz oriental en Iran. *Ecolage Geol. Helv.* 71, 551–580.
- Johnson, P.R., 2014. An expanding Arabian–Nubian Shield geochronologic and isotopic dataset: defining limits and confirming the tectonic setting of a Neoproterozoic accretionary orogen. *Open Geol. J.* 8, 3–33.
- Kobyliński, C., Hattori, K., Smith, S., Plouffe, A., 2020. Protracted magmatism and mineralized hydrothermal activity at the Gibraltar porphyry copper-molybdenum deposit, British Columbia. *Econ. Geol.* 115 (5), 1119–1136.
- Kolodner, K., Avigad, D., McWilliams, M., Wooden, J.L., Weissbrod, T., Feinstein, S., 2006. Provenance of north Gondwana Cambrian–Ordovician sandstone: U–Pb SHRIMP dating of detrital zircons from Israel and Jordan. *Geol. Mag.* 143, 367–391.
- Legault, M.L., Hattori, K., 1994. Provenance of igneous clasts in conglomerates of the Archaean Timiskaming Group, Kirkland Lake area, Abitibi greenstone belt, Canada. *Can. J. Earth Sci.* 31, 1749–1762.
- Ludwig, K.R., 2012. User's Manual for ISOPLOT 3.75: A Geochronological Toolkit for Microsoft Excel. Berkeley Geochronology Center, Special Publication 5, Berkeley, California, p. 75.
- Meinhold, G., Morton, A.C., Avigad, D., 2013. New insights into peri-Gondwana paleogeography and the Gondwana super-fan system from detrital zircon U–Pb ages. *Gondwana Res.* 23, 661–665.
- Metcalfe, I., 2013. Gondwana dispersion and Asian accretion: Tectonic and palaeogeographic evolution of eastern Tethys. *J. Asian Earth Sci.* 66, 1–33.

- Moghadam, H.S., Griffin, W.L., Li, X.-H., Santos, J.F., Karsli, O., Stern, R.J., Ghorbani, G., Gain, S., Murphy, R., O'Reilly, S.Y., 2017a. Crustal evolution of NW Iran: Cadomian arcs, Archean fragments and the Cenozoic magmatic flare-up. *J. Petrol.* 58, 2143–2190.
- Moghadam, H.S., Li, X.H., Griffin, W.L., Stern, R.J., Thomsen, T.B., Meinhold, G., Aharipour, R., O'Reilly, S.Y., 2017b. Early Paleozoic tectonic reconstruction of Iran: tales from detrital zircon geochronology. *Lithos* 268–271, 87–101.
- Mongelli, G., Boni, M., Buccione, R., Sinisi, R., 2014. Geochemistry of the Apulian karst bauxites (southern Italy): chemical fractionation and parental affinities. *Ore Geol. Rev.* 63, 9–21.
- Mongelli, G., Buccione, R., Gueguen, E., Langone, A., Sinisi, R., 2016. Geochemistry of the Apulian allochthonous karst bauxite, Southern Italy: distribution of critical elements and constraints on Late Cretaceous Peri-Tethyan palaeogeography. *Ore Geol. Rev.* 77, 246–256.
- Morag, N., Avigad, D., Gerdes, A., Belousova, E., Harlavan, Y., 2011. Crustal evolution and recycling in the northern Arabian-Nubian Shield: new perspectives from zircon Lu-Hf and U-Pb systematics. *Precambrian Res.* 186, 101–116.
- Muttoni, G., Mattei, M., Balini, M., Zanchi, A., Gaetani, M., Berra, F., 2009a. The drift history of Iran from the Ordovician to the Triassic. In: Brunet, M.F., Wilmsen, M., Granath, J. (Eds.), *South Caspian to Central Iran Basins*. *Geol. Soc. Lond. Spec. Publ.* vol. 312, pp. 129–160.
- Muttoni, G., Gaetani, M., Kent, D.V., Sciunnach, D., Angiolini, L., Berra, F., Garzanti, E., Mattei, M., Zanchi, A., 2009b. Opening of the Neo-Tethys Ocean and the Pangea B to Pangea A transformation during the Permian. *Geotitles* 14, 17–48.
- Ramezani, J., Tucker, R.D., 2003. The Saghand Region, Central Iran: U-Pb geochronology, petrogenesis and implications for Gondwana tectonics. *Am. J. Sci.* 303, 622–665.
- Renaud, K.M., Wardlaw, B.R., Hubbard, B.E., 2015. Assessment of bauxite, clay, and laterite deposits in Afghanistan. U.S. Geological Survey Open-File Report 2014–1210, p. 40 <https://doi.org/10.3133/ofr20141210>.
- Robert, A.M.M., Letouzey, J., Kavooosi, K.A., Sherkat, Sh., Müller, C., Vergés, J., Aghababaei, A., 2014. Structural evolution of the Kopeh Dagh fold-and-thrust belt (NE Iran) and interactions with the South Caspian Sea Basin and Amu Darya Basin. *Mar. Petrol. Geol.* 57, 68–87.
- Rubatto, D., 2002. Zircon trace element geochemistry: distribution coefficients and the link between U-Pb ages and metamorphism. *Chem. Geol.* 184, 123–138.
- Santosh, M., Maruyama, S., Yamamoto, S., 2009. The making and breaking of supercontinents: Some speculations based on superplumes, super downwelling and the role of tectosphere. *Gondwana Res.* 15, 324–341.
- Seeger, F.E., 1977. *Zur Geologie des Nord-Alamut Gebietes (Zentral-Elburz)*. PhD Thesis. Eidgenössische Technische Hochschule, Zurich, p. 161.
- Sengör, A.M.C., 1979. Mid-Mesozoic closure of Permo-Triassic Tethys and its implications. *Nature* 279, 590–593.
- Sengör, A.M.C., 1987. Tectonics of the Tethysides: orogenic collage development in a collisional setting. *Annu. Rev. Earth Planet. Sci.* 15, 213–244.
- Seyed-Emami, K., Fürsich, F.T., Wilmsen, M., Majidifard, M.R., Cecca, F., Schairer, G., Shekarifard, A., 2006. Stratigraphy and ammonite fauna of the upper Shemshak Formation (Toarcian–Aalenian) at Tazareh, eastern Alborz, Iran. *J. Asian Earth Sci.* 28, 259–275.
- Shirdashtzadeh, N., Torabi, G., Schaefer, B., 2018. A magmatic record of Neoproterozoic to Palaeozoic convergence between Gondwana and Laurasia in the northwest margin of the Central-East Iranian Microcontinent. *J. Asian Earth Sci.* 166, 35–47.
- Stampfli, G.M., 1978. *Etude géologique générale de l'Elbourz oriental au sud de Gonbad-e Qabus, Iran NE*. PhD thesis. Université de Genève, p. 315.
- Stampfli, G.M., 2000. Tethyan oceans. In: Bozkurt, E., Winchester, J.A., Piper, J.D.A. (Eds.), *Tectonics and Magmatism in Turkey and Surrounding Area*. *Geol. Soc. Lond. Spec. Publ.* vol. 173, pp. 1–23.
- Stampfli, G.M., Marcoux, J., Baud, A., 1991. Tethyan margins in space and time. *Palaeogeogr. Palaeoclimatol. Palaeoecol.* 87, 373–409.
- Stern, R.J., 2002. Crustal evolution in the East African Orogen: a neodymium isotopic perspective. *J. Afr. Earth Sci.* 34, 109–117.
- Stern, R.J., Johnson, P., 2010. Continental lithosphere of the Arabian Plate: a geologic, petrologic, and geophysical synthesis. *Earth Sci. Rev.* 101, 29–67.
- Stöcklin, J., 1968. Structural history and tectonics of Iran: a review. *Am. Assoc. Pet. Geol. Bull.* 52, 1229–1258.
- Ueno, K., 2003. The Permian fusulinoid faunas of the Sibumasu and Baoshan blocks: their implications for the paleogeographic and paleoclimatologic reconstruction of the Cimmerian Continent. *Palaeogeogr. Palaeoclimatol. Palaeoecol.* 193, 1–24.
- Ustaömer, P.A., Ustaömer, T., Collins, A.S., Robertson, A.H.F., 2009. Cadomian (Ediacaran–Cambrian) arc magmatism in the Bitlis Massif, SE Turkey: magmatism along the developing northern margin of Gondwana. *Tectonophysics* 473, 99–112.
- Wang, Q., Deng, J., Liu, X., Zhao, R., Cai, S., 2016. Provenance of Late Carboniferous bauxite deposits in the North China Craton: new constraints on marginal arc construction and accretion processes. *Gondwana Res.* 38, 86–98.
- Watson, E.B., Harrison, T.M., 1983. Zircon saturation revisited: temperature and composition effects in a variety of crustal magma types. *Earth Planet. Sci. Lett.* 64, 295–304.
- Wilmsen, M., Fürsich, F.T., Seyed-Emami, K., Majidifard, M.R., Taheri, J., 2009. The Cimmerian Orogeny in northern Iran: tectono-stratigraphic evidence from the foreland. *Terra Nova* 21, 211–218.
- Yu, W., Algeo, T.J., Du, Y., Zhang, Q., Liang, Y., 2016. Mixed volcanogenic–lithogenic sources for Permian bauxite deposits in southwestern Youjiang Basin, South China, and their metallogenic significance. *Sediment. Geol.* 341, 276–288.
- Zamanian Pedram, M., Karimi, H.R., 2007. *Geological Map of Aliabad (Scale 1:100,000)*. Geological Survey of Iran, Tehran.